


Time course of cytochrome oxidase blob plasticity in the primary visual cortex of adult monkeys after retinal laser lesions

Mariana F. Farias¹ | Leslie G. Ungerleider³ | Sandra S. Pereira² |
Ana Karla J. Amorim¹ | Juliana G. M. Soares¹ | Ricardo Gattass¹ 

¹Laboratory of Cognitive Physiology, Instituto de Biofísica Carlos Chagas Filho, UFRJ, Rio de Janeiro, RJ, Brazil

²Department of Ophthalmology, School of Medicine, UFRJ, Rio de Janeiro, RJ, Brazil

³Laboratory of Brain and Cognition, National Institute of Mental Health, National Institutes of Health, Bethesda, Maryland

Correspondence

Ricardo Gattass, Institute of Biophysics Carlos Chagas Filho, Bloco G, CCS, Rio de Janeiro, RJ 21941 Brazil.
Email: rgattass@gmail.com

Funding information

Financiadora de Estudos e Projetos, Grant/Award Number: PEC 20150; Fundação Carlos Chagas Filho de Amparo à Pesquisa do Estado do Rio de Janeiro, Grant/Award Number: E-26/210.917/2016, E-26/110.905/2013; Conselho Nacional de Desenvolvimento Científico e Tecnológico, Grant/Award Number: 471.166/2013-8; NIH Z01 MH002035-28

Abstract

We studied the time course of changes of cytochrome oxidase (CytOx) blob spatial density and blob cross-sectional area of deprived (D) and nondeprived (ND) portions of V1 in four capuchin monkeys after massive and restricted retinal laser lesions. Laser shots at the border of the optic disc produced massive retinal lesions, while low power laser shots in the retina produced restricted retinal lesions. These massive and restricted retinal lesions were intended to simulate glaucoma and diabetic retinopathy, respectively. We used a Neodymium-YAG dual frequency laser to make the lesions. We measured Layer III blobs in CytOx-reacted tangential sections of flat-mounted preparations of V1. The plasticity of the blob system and that of the ocular dominance columns (ODC) varied with the degree of retinal lesions. We found that changes in the blob system were different from that of the ODC. Blob sizes changed drastically in the region corresponding to the retinal lesion. Blobs were larger and subjectively darker above and below the non deprived ODC than in the deprived columns. With restricted lesions, blobs corresponding to the ND columns had sizes similar to those from non-lesioned areas. In contrast, blobs corresponding to the deprived columns were smaller than those from nonlesioned areas. With massive lesions, ND blobs were larger than the deprived blobs. Plastic changes in blobs described here occur much earlier than previously described.

KEYWORDS

blob, ocular dominance column, modular organization, striate cortex, V1

1 | INTRODUCTION

The primary visual cortex, also named striate cortex, area 17 of Brodmann or visual area 1 (V1), is the first of a series of visual areas, located in the posterior and medial portions of the occipital lobe. In 1979, Wong-Riley used the histochemistry for cytochrome c oxidase (CytOx), a mitochondrial enzyme of oxidative metabolism, to map functional activity in V1 (Wong-Riley, 1979). Horton & Hubel (1981) studied the tangential organization of clusters of cells rich in CytOx in the cortical layers in V1 of macaque monkey. They showed that some columns are more reactive than neighboring columns in all cortical layers, except for Layer IV. In sections tangential to the cortical surface, mainly in Layers

II and III, these columns appear as a regular arrangement of rich round or oval stains in CytOx, with a 180–250 μm diameter and a center-to-center spacing of 300–600 μm (Trusk et al., 1990). These structures received different terms: “patches” (Horton & Hubel, 1981, Marcondes et al., 2018, Wong-Riley & Carroll, 1994), “blobs” (Farias et al., 1997; Lachica et al., 1992; Livingstone & Hubel, 1982;), “spots” (Tootell et al., 1985), “puffs” (Carroll & Wong-Riley, 1984) or “dots” (Hendrickson, 1985). Thus, the blobs appear as CytOx-rich areas, organized in arrays, and each one in registration with ocular dominance columns (ODC) in Layer IVc. The arrays of blobs are perpendicular to the pial surface.

LeVay et al. (1985) described the pattern of ODC in macaque monkeys. In the macaque, Horton (1984) found that deprived CytOx blobs

This is an open access article under the terms of the Creative Commons Attribution-NonCommercial License, which permits use, distribution and reproduction in any medium, provided the original work is properly cited and is not used for commercial purposes.

© 2018 The Authors The Journal of Comparative Neurology Published by Wiley Periodicals, Inc.

decrease their cross-sectional area while ND blobs at the representation of the retinal lesion do not alter their size. Later, Trusk & Wong-Riley (1991) observed, in macaques submitted to unilateral retinal lesions, an increase in CytOx reactivity in the region located between the blobs overlying the stripes of the intact eye, as compared with normal tissue. In a study of enucleated adult *Sapajus apella* (formally *Cebus apella*) monkeys, Rosa et al. (1988, 1992) found many similarities of the ODC system to those described by LeVay et al. (1985). Rosa et al. (1991) showed that deprived V1 blobs had a decreased cross-sectional area in Layer III, while ND blobs in the same region had an increased cross-sectional area.

To clarify discrepancies in the literature regarding the effects of visual deprivation on the time course of plastic changes in blobs, we studied the CytOx pattern in V1 of adult capuchin monkeys after either focal (restricted) lesions of the retina or lesions of the margin of the optic disc (massive). Massive lesions simulated lesions resulting in glaucoma, while restricted, focal lesions simulated diabetic retinal lesions, which have distinct involvement of ganglion cell axons. Restricted lesions barely affect retinal fibers, while massive lesions destroy most retinal fibers. In this study, unlike previous ones, we used sequential small or large retinal laser lesions to study the time course of plasticity of ODC and CytOx rich blobs in flattened preparations of V1. We also determined whether plasticity of the blobs in the two lesion conditions occurs only by retraction of the deprived blobs or occurs by both retraction of the deprived blobs and expansion of the ND ones.

2 | METHOD

Four adult male *Sapajus apella* (formerly *Cebus apella*) monkeys, weighing between 3 and 4 kg, were used. The procedures and protocols followed the NIH guidelines for Use of Laboratory Animals. The IBCCF/UFRJ research committee approved these procedures. Using a hand-held ophthalmoscope, we examined the fundi of the eyes to ensure that there was no previous lesion in the retinas of the animals.

2.1 | Retinal lesions

Before each session of retinal lesion, the animals were anesthetized with 1.5 ml of a mixture of four parts of ketamine (6% Ketalar, Parke-Davis) for one part of xylazine hydrochloride (2% Rompun, Bayer). A mixture of 0.6 ml of atropine sulfate (Atropina, Hypofarma, 0.15 mg/kg) and 0.4 ml of Diazepam (Valium, Roche, 0.8 mg/kg) was injected to prevent tracheobronchic secretion and stress. Two drops of the ophthalmic solutions of 10% phenylephrine hydrochloride (10% Fenilefrina, Oculum) and tropicamide (1% Mydríacyl, Alcon) were applied to the animals' eyes to dilate the pupil and facilitate visualization of the fundus of the eye. Local anesthetic (Tetracaine Hydrochloride 100 mg-Allergan-Frumtost) was applied to the cornea. Soon after, a lens OMRA-WF Mainster Wide Field (Ocular Instruments, Inc.) with objective of 5× soaked in a solution of 2% methylcellulose was positioned onto the cornea of the animal. This lens allowed visualization of the posterior pole and equator, and of the retinal periphery (Medeiros, 1997). The lesions of the retinas were made at different times relative

to the time of euthanasia. These lesions were induced by photocoagulation with a Neodymium Laser (OPHTHALAS 532 nm) mounted to a rift ophthalmoscope (Top-Con AIT-20, Carl Zeiss 30 SL-M). Neodymium (Nd): Yttrium aluminum garnet (YAG) double frequency laser (OPHTHALAS) has a nonlinear krypton-titanium-phosphate crystal, which can transform the radiation of 1064 nm of the Laser Nd:YAG in 532 nm, producing a green monochrome wave. Nd:YAG (neodymium-doped yttrium aluminum garnet, Nd:Y3Al5O12) is a crystal that is used as a lasing medium for solid-state lasers. The infrared radiation emitted by the Nd:YAG laser crosses the eye without being absorbed by the cornea. The wavelength of this laser (532 nm) is well absorbed by melanin and hemoglobin, but has little absorption by the macular xanthophyll's (Barsante & Diniz, 1997; Bozinis, 1997).

High-power laser shots destroy all retinal layers and sever fibers of passage in the inner layers of the retina, while low-power laser shots disrupt the retinal structure by destroying the outer retinal layers. Lesions to the optic disc produce a devastating effect on fibers of passage, resulting in larger scotoma than similar lesions in other portions of the retina. Similar shots in the retina destroy photoreceptors and have a much smaller effect on fibers of passage. The degree of plasticity in the cortex depends on the location and amount of energy of the laser shots.

We used two different paradigms, one with focal lesions with laser shots on the retina and the other with massive lesions with laser shots on the margin of the optic disc. Restricted, focal lesions barely affect the retinal fibers, while massive lesions have a large effect on ganglion cell axons and destroy most retinal fibers (Figure 1). The first paradigm illustrated in Figure 2 is based on multiple low power laser shots to the retina at similar eccentricities done at different times before euthanasia. This figure is a schematic illustration of the restricted retinal lesion paradigm used in Cases CD4 and CD5. The resultant ODC appear on the flattened representations in V1 on the areas corresponding to the retinal lesions. Four rows of laser shots (0.3 mv, 0.2 s), at different eccentricities, were made in different visual quadrants in each retina, namely, the superior quadrant of the temporal hemifield in the right retina and the inferior quadrant of the temporal hemifield in the left retina. The lesions were made starting from the periphery of the retina (older lesions) and ending at more central regions (more recent lesions). This procedure avoided destroying fibers of passage that could mask deafferentation of control regions of the retina. The earlier lesions were made 42 days (case CD4) or 40 days (case CD5) before euthanasia; subsequent lesions were made at 27, 13, and 3 days in both cases. After all the lesions were made, fundus photographs were taken with a fundus camera (Top-Con TRC-50 WENT Retinal Camera) coupled to a CCD video camera. Figure 3 shows the fundus photography of the left eye of case CD5 after the last lesion.

We used the massive lesion paradigm in Cases DO1 and DO2. These lesions were made with laser shots (0.8 mv, 0.2 s) at the border of the right optic disc, at different times before euthanasia; 25, 3 and 1 day in case DO1 and 52 and 2 days in case DO2. The lesions destroyed fibers of passage coming from large portions of the retina. Figure 4 shows schematic diagrams of the massive lesion paradigm used in Case DO1. The areas of the right retina with ganglion cells degeneration

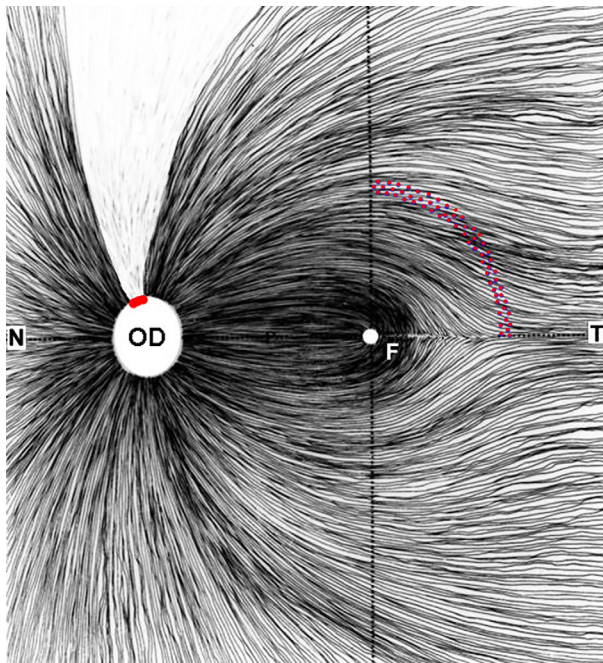


FIGURE 1 Schematic diagram illustrating the lesion locations superimposed on the retinal fiber track. Massive lesions were obtained by laser shots at the border of the optic disc, while restricted lesions were generated by small laser shots at the retina. Virtually no degeneration of axons is observed after minor laser lesions of the retina. Note the ganglion cell axons degeneration after the optic disc laser lesions. Red circles represent laser shots. Abbreviations: OD, optic disc; F, fovea; N, nasal retina; T, temporal retina. Massive lesions were inspired by the lesion present in glaucoma, while discrete, restricted lesions were inspired diabetic retinal lesions [Color figure can be viewed at wileyonlinelibrary.com]

involved almost the entire visual field representation, sparing only the central lower field representation. These lesions resulted in deafferented regions of left (LH) and right (RH) hemispheres with the appearance of ODC at the cortical representation of V1 seen at the flattened preparations of Layer IV.

2.2 | Flattened maps

After the stipulated survival times, the animals received lethal doses of sodium pentobarbital (100 mg/kg, IV) and were transcardially perfused with 0.9% saline. The eyes of the animals were removed, cut at the equator and photographed with the aid of a CCD camera on a Nikon stereomicroscope. Figure 5 presents a photograph of the posterior pole of the right eye of case DO2, showing the results of laser lesions at the border of the optic disc. The limits between the lesions made at 52 and 2 days are indicated by asterisks and the nonaffected nasal border is between arrows. Photographs of the posterior pole of the right eyes of cases CD4 and CD5 with the scars of the lesions made at 3, 13, 27, and 40 or 42 days are shown in Figure 6.

In cases CD4 and CD5, the eye cups with the retina were dehydrated, embedded in paraffin, and cut at a thickness of 15 μ m (CD4) or 10 μ m (CD5). The sections were mounted on glass slides, defatted and

stained with hematoxylin and eosin. Figure 7 illustrates a section of the retina of case CD5 stained with hematoxylin-eosin, on which the intact regions of the retina, the optic disc and the optic nerve can be seen. A section of the retina with a small lesion is shown below.

In order to obtain flat-mounts of V1, the brain was removed from the skull and the posterior portion underwent the flat-mounting procedure described by Tootell & Silverman (1985, Method II). Flat-mounted blocks were fixated between parafilm-covered glass slides with a solution of 4% paraformaldehyde in 0.1 M phosphate buffer for 6 hr, followed by 4% paraformaldehyde/10% sucrose and paraformaldehyde/30% sucrose for 3 hr. Then the blocks were kept overnight in PBS/30% sucrose. After fixation, the blocks were quickly frozen and cut at 40 μ m in a freezing microtome. The CytOx histochemical reaction followed the protocol of Wong-Riley (1979), as modified by Silvermann and Tootell (1987). Sections stained for CytOx were photographed under blue light illumination using high contrast film (KodalithTM, Kodak Co.).

The use of CytOx histochemistry allows the visualization of OD stripes in Layer IV of V1 and, indirectly, the limits of the representative area of the retinal lesion. The extent of the lesion was determined by correlating the limits of the lesion, as revealed by the ODC in V1, to the visuotopic map of V1, proposed by Gattass et al. (1987).

A quantitative analysis of the CytOx blobs was performed in sections nearly tangential to Layer III of flattened preparations of V1 and surrounding areas. We chose to analyze blob topography at the mid-portion of Layer III, which shows the highest contrast between CytOx-rich and CytOx-poor tissue. Reconstruction of CytOx blobs was accomplished by superimposing photographs of serial sections using blood vessels as landmarks.

The stained sections were photographed with high contrast film (KodalithTM, 12 ASA) in a Leitz Aristophot. The negatives were enlarged 7 \times and copied onto standard Kodabromide photographic paper. We made manual photographic reconstructions of ODC and blobs in the three animals and digital reconstructions in case CD4. Manual reconstruction was made starting from the cutting, assembly and collage of pieces of photos of the several sheets. At the end, there were four reconstructions of V1 for each case: one for the blobs of CytOx and another of ODC for both hemispheres. Manual photographic reconstructions of ODC and blobs are shown in Figures 8 (case CD5) and 9 (cases DO1 and DO2).

In the digital reconstructions, the enlarged photos of the stained sections were digitalized in a table scanner (Scan Jet 2600C, HP) and the reconstruction of the cortical layers was made in Photoshop 5.0 using a PC-computer. The four digital reconstructions of case CD4 are illustrated in Figure 10.

In the manual reconstructions, the blobs and ODC were delineated manually in a transparent sheet with the aid of a fine-point pen. The transparency sheets with the two groups of delineated blobs, one group in register with the deprived ODC (deprived blobs) and the other in register with the nondeprived ODC (nondeprived blobs), were then digitized (Scan Jet 2600C-HP) and the size of each blob was measured with the aid of the program ScnImage (Axion, CO). The size of the blobs in the control areas of the cortex, where there was no corresponding lesion, was also measured.

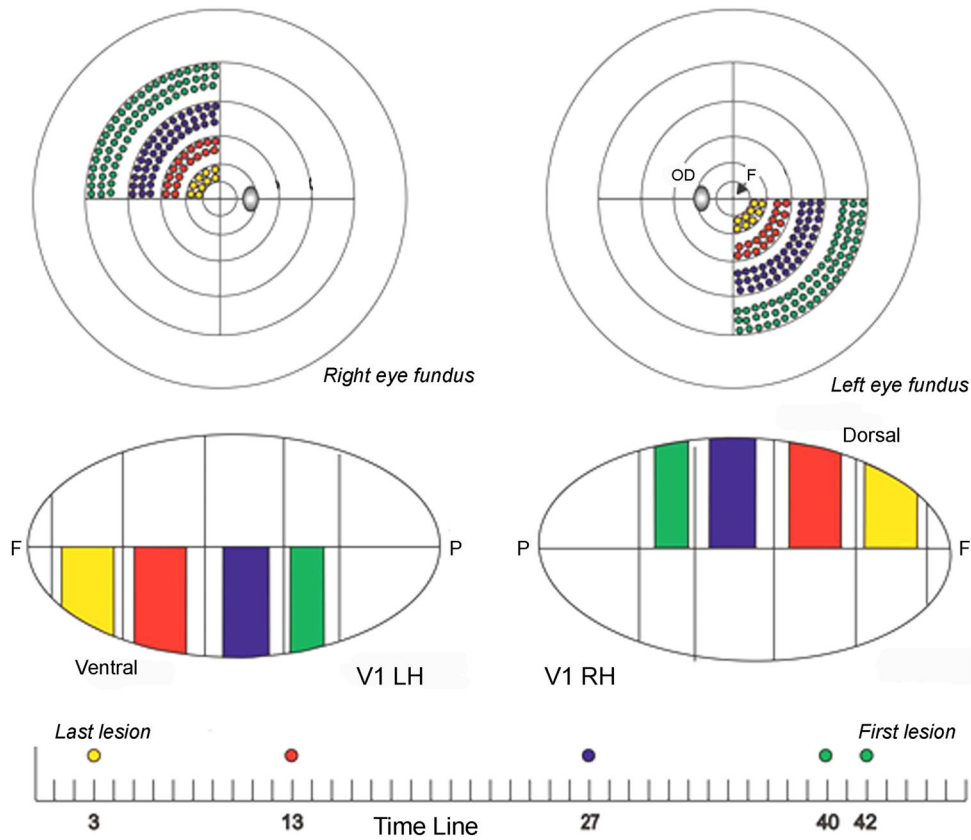


FIGURE 2 Schematic diagram of the restricted retinal lesion paradigm used in Cases CD04 and CD05. Top: Right and left schematic representations of the retinas showing four strips of laser shots at different eccentricities, made at different times. Middle: Flattened representations of the areas corresponding to the retinal lesions in the left (LH) and right (RH) hemispheres in V1. F, fovea and P, periphery. Bottom: Timeline of the lesions. The earlier lesions (40–42 days) were located peripherally, while the later lesions (3 days) were more central

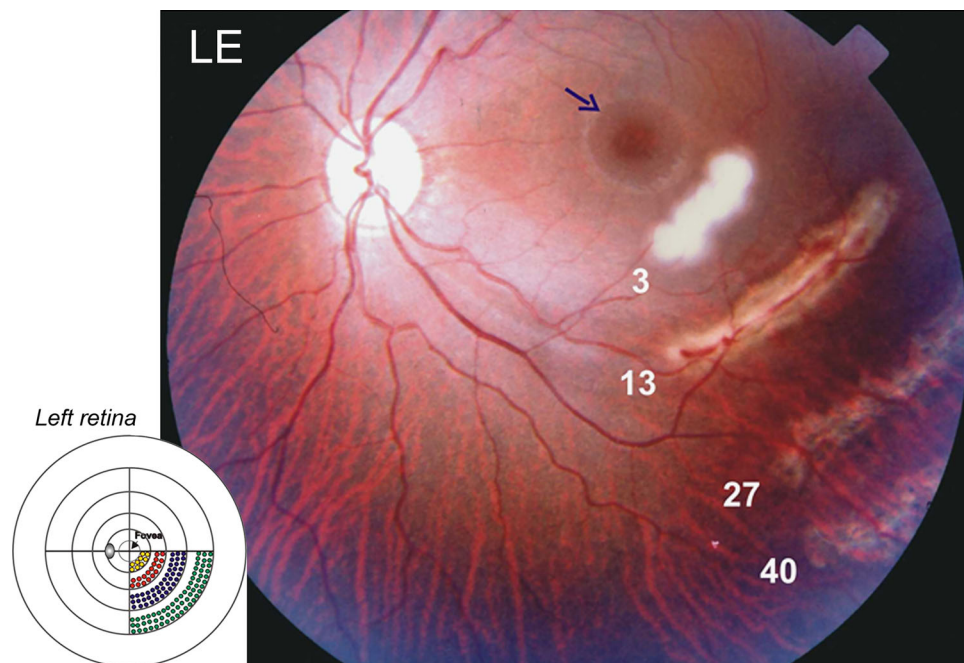


FIGURE 3 Fundus photograph of the left eye after the last retinal lesion (3 days) in Case CD5. Lower left insert: representation of the fundus of the left eye showing the lesions at different days before euthanasia. Note that the restricted lesions (40, 27, 13, and 3) show unusual amounts of fibrosis and edema. Blue arrow points to the foveola

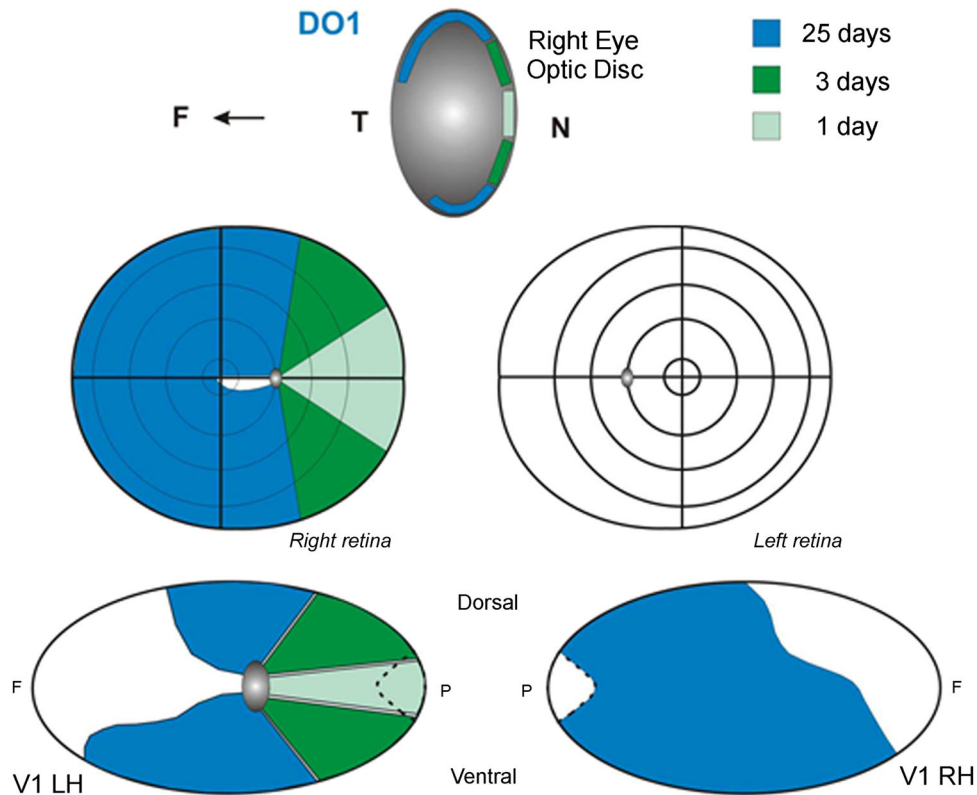


FIGURE 4 Schematic diagrams of the massive lesion paradigm used in Cases DO1. Top: Lesions made at the border of the right optic disc at different times. Middle: Representation of the areas of the right retina with ganglion cell degeneration. Bottom: Cortical representation of the flattened preparations of V1 showing the deafferented areas of left (LH) and right (RH) hemispheres. Different colors represent lesions at the optic disc in the different times and its projections for the retinal (middle) and cortical (bottom) levels

2.3 | Blob measurements

At the start of this study, an evaluation of the borders of the blobs was performed by an automated digital image processing system and a semi-automated system based on the subjective delineation of the border by different experimenters to match a standard template. Examples of subjective delineation of blobs have been shown previously (Rosa et al., 1991; Farias et al., 1997). A standard template was determined with the aid of the automated image processing system after filtering the image with a 2D-rolling ball algorithm to normalize the contrast, setting the contrast threshold that subjectively matched the appropriate blob size, and eliminating the false blobs due to histological and blood vessels artifacts. The subjectivity of the steps involved in the automated process and the occasional variation of the staining of large areas of the cortex required the use of the semi-automated method. Thus, for the quantitative analysis, blobs were outlined with a fine-point permanent marker on enlarged (5×) contrast-matched prints of each section. The outlined blobs were then scanned and measured with the aid of a computer program (ImageJ, courtesy NIH). This program also provided the size and the X-Y coordinates of the center of the blob (centroid) used to calculate the spatial density of the blobs. The density was determined by two methods. First, the number of blobs in a test square of one square millimeter was counted in every region of V1 where all blobs were visible. Second, the mean density was calculated using the nearest neighbor analysis of blob centroids. There was no statistical difference

in measurements performed in the same hemisphere by two different experimenters, indicating negligible differences introduced by having different experimenters analyze the data. Nonetheless, for any given case, the measurements presented were performed by at least two

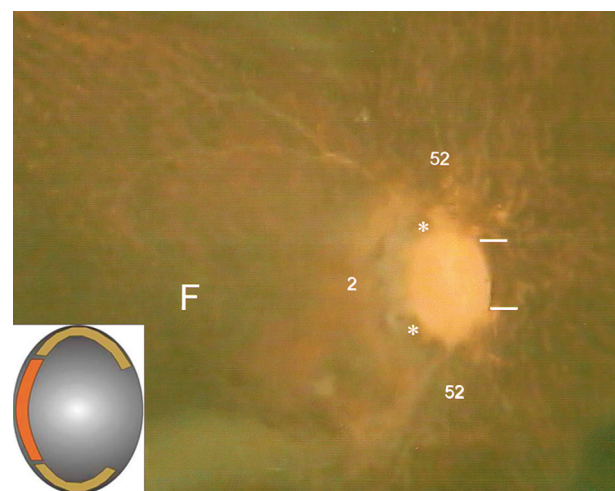


FIGURE 5 Photograph of the posterior pole of the right eye showing the results of laser lesions at the border of the optic disc in Case DO2. Non-lesioned nasal border is between white lines, while the limits between the lesions made at 52 and 2 days are indicated by asterisks. For details, see text

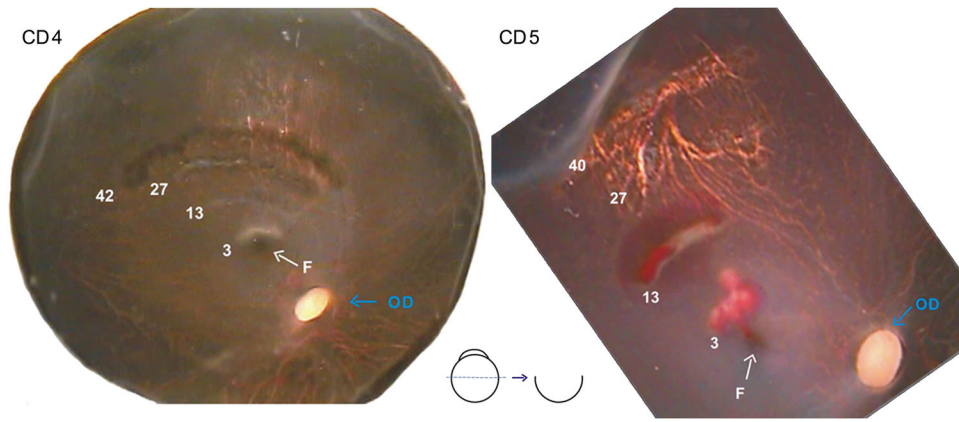


FIGURE 6 Photography of the posterior pole of the right eyes of Cases CD4 and CD5. Blue arrows indicate the optic discs (OD), and white arrows point to the fovea (F). Scars of the lesions are labeled by their age (3, 13, 27, 40, and 42 days). Insert at lower left indicates the level of the cut of the eyes [Color figure can be viewed at wileyonlinelibrary.com]

observers. Therefore, the occasional fuzziness of blob boundaries did not appear to interfere with our analysis of blob sizes.

3 | RESULTS

In the current study, we prepared capuchin monkeys with either massive or restricted retinal lesions in order to simulate conditions present in glaucoma and diabetic retinopathy, respectively. We then examined the effects of these lesions on the CytOx-rich blobs and ODCs in in V1.

We analyzed two kinds of CytOx blobs, one in register with the ND, darkly stained ODCs and the other in register with the deprived, lightly stained ODCs, in flattened preparations of Layer III. Blobs in normal areas of V1, corresponding to nonlesioned retina, were also analyzed. We measured the size and the number of blobs per mm² at the regions of representation of the different timed lesions, at Layer III where they are better delineated throughout V1. In all cases, and for all timed lesions, there was a significantly greater ($p < .0001$) decrease in blob size for bobs located above the deprived ODCs compared to both control and ND blobs, but variations in blob size and density depended on the type and time of the lesions.

Flattened reconstructions of Layer IVc of CytOx reacted V1 showing ODCs and reconstructions of Layer III showing blob characteristic and topography are shown in Figures 8–10. Figures 8 and 10 show the effect of focal lesion on the retina in cases CD5 and CD4. Figure 9 shows the effect of massive lesions caused by laser shots on the margin of the optic disc in cases CD1 and CD2. Lesions at the optic disc produce a devastating effect on fibers of passage, resulting in larger scotoma than similar lesions in other portions of the retina (compare Figure 9 with Figures 8 and 10).

3.1 | Restricted lesions – cases CD4 and CD5

The top of Figure 11 illustrates the size of the control (C), deprived (D) and ND blobs for the different timed lesions in cases CD4 and CD5. The size of the deprived blobs was significantly smaller than that of the

control ($p < .0001$) for all timed lesions, with a decrease to 30% (CD5) or 44% (CD4) of the control size at 3 days post-lesion and continuing to decrease at 13 days post-lesion ($p < .4$). After that, their reduced size was maintained at 42 days post-lesion, but there was no significant size difference among 13, 27, and 42 days post-lesion. The ND blobs did not show significant size variations at any of the post-lesion time-points.

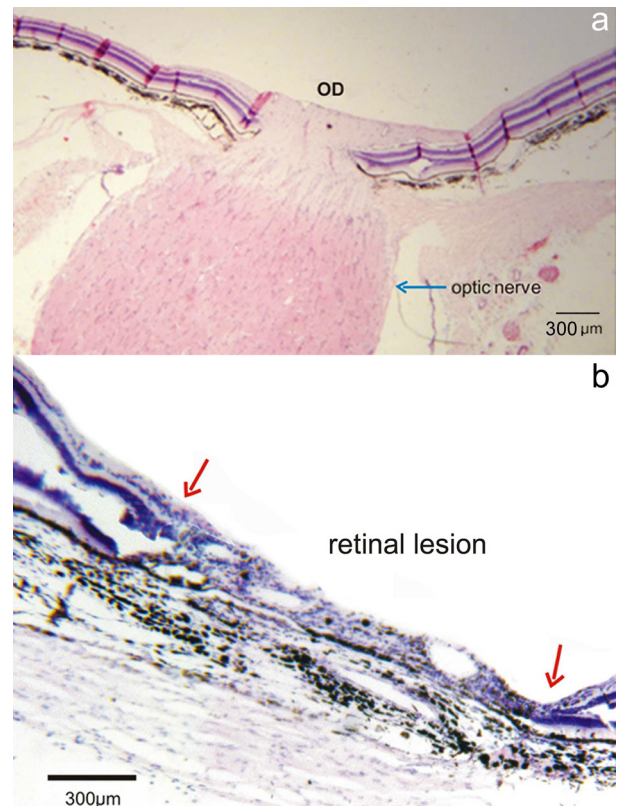


FIGURE 7 Photomicrographs of sections of the retina stained for hematoxylin-eosin in Case CD5. (a) Section showing part of the intact retina, the optic disc and the optic nerve. (b) Section of the retina showing a small retinal lesion. The arrows indicate the borders of the lesion

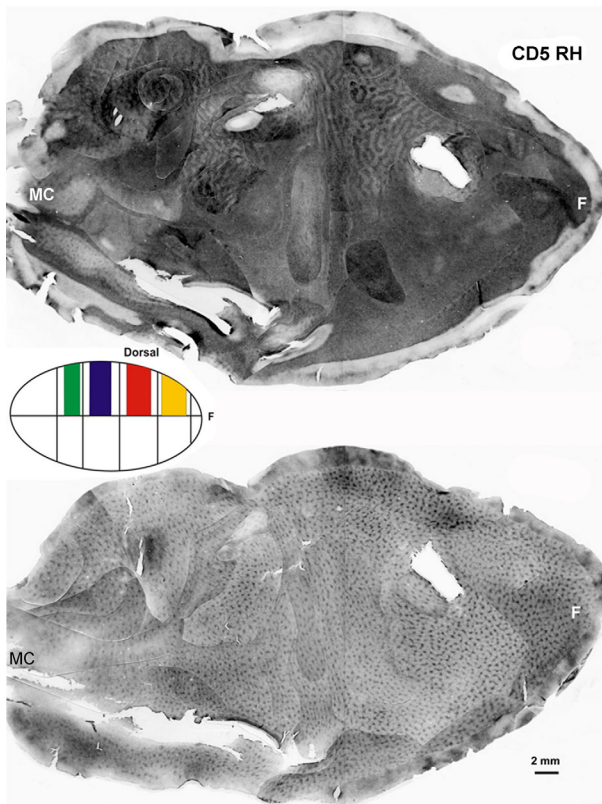


FIGURE 8 Photographic reconstructions of ocular dominance columns (ODC) in layer IVc (top) and blobs in Layer III (bottom) of V1 of the right hemisphere (RH) in Case CD5. The small drawing (middle) is a schematic diagram of the lesioned areas in this case. The lesions resulted in a pattern of ODC in V1, corresponding to the topographical location of the lesions. (F, fovea, MC, monocular crescent). See also the legend for Figure 2 [Color figure can be viewed at wileyonlinelibrary.com]

The deprived blob density (blobs/mm²) was significantly lower ($p < .0001$) than the ND blob density at all post-lesion time-points. The blob density continued decreasing to 13 days post-lesion ($p < .005$) and remained reduced at 42 days post-lesion, but, like the blob size, it did not differ significantly at 13, 27, and 42 days post-lesion. The ND blob density did not differ significantly among any of the post-lesion time-points (Figure 12b).

Thus, in cases with restricted lesions, we observed a decrease in both size and density of the deprived blobs at 3 days post-lesion, and this decrease continued to 13 days post-lesion, with a decrease of 20–25% of the control blob size. Both blob size and density stabilized at 42 days post-lesion. There was no variation in blob size or density in ND regions of V1.

3.2 | Massive lesions – cases DO1 and DO2

The size of the control (C), deprived (D) and ND blobs at the different post-lesion time-points in cases DO1 and DO2 are illustrated at the bottom of Figure 11. In these cases, the size of the blobs in deprived regions of V1 was significantly smaller than in control regions ($p < .0001$) at all post-lesion time-points. They decreased in size to 45%

of the control size at first day post-lesion in case DO1 and to 28% of the control size at 2 days post-lesion in case DO2. In case DO1 there was no significant difference in the size in deprived V1 blobs among the post-lesion time-points; in case DO2, however, the deprived blobs increased in size from 2 (28% of control size) to 52 days (33% of control size) post-lesion. In these cases with massive lesions, the ND blobs size increased at 2 days post-lesion (108% of the control size, $p < .007$) and increased to 120% of the control size at 29 days post-lesion in case DO1 and 55 days post-lesion in case DO2 ($p < .0001$).

The deprived blob density (blobs/mm²) was significantly smaller ($p < .0001$) than the ND blob density at all post-lesion time-points. We did not observe a significant difference in blob density among the post-lesion time-points (Figure 12a).

3.3 | Time course of blob plasticity

The plastic changes described here were observed 2–3 days after the lesions. These blob changes depended on the severity of the visual deafferentation and of the survival time of the animal. The results suggest the existence of two different mechanisms: one of shrinkage of the deprived blobs that occurs in the first days post-lesion and another, more subtle, of expansion of the ND blobs that occurs after 25 days post-lesion in animals with massive lesions.

Figure 13 shows changes in blob size over time after restricted (cases CD4 and CD5) and massive (cases DO1 and DO2) retinal lesions. There was a large difference in blob size: limited deafferentation of V1, caused by a set of small focal lesions, decreased the size and density of deprived V1 blobs at 3 days post-lesion, which stabilized at 13 days post-lesion, while massive deafferentation of V1, caused by widespread axonal injury, caused a greater decrease of deprived blob size and density at 2 days post-lesion.

Figure 13 also shows an expansion in blob cross-sectional areas of ND blobs in cases with massive retinal lesions.

4 | DISCUSSION

Enucleation studies (Horton & Hubel, 1981; Horton, 1984; Hendrickson, 1985; Trusk et al., 1990), ion channel blockage with tetrodotoxin (TTX) (Wong-Riley & Carroll, 1984; Wong-Riley et al., 1989; Trusk et al., 1990) and eyelid suture (Hendry & Jones, 1986; Horton, 1984; Trusk et al., 1990) reduce the reactivity of CytOx in deprived V1 blobs in register with ODCs corresponding to the affected eye. This loss of reactivity indicates that the high activity of CytOx in the normal blobs depends on only the functional afferents of the intact eye, thus demonstrating the occurrence of metabolic plasticity in cortical neurons in the mature brain (Trusk et al., 1990).

Monocular treatments in which the retinal afferents are totally interrupted, as in cases of enucleation or TTX injection, cause a fast loss of CytOx activity in the deprived blobs (Wong-Riley & Carroll, 1984; Wong-Riley et al., 1989; Trusk et al., 1990). On the other hand, monocular deprivation with eyelid suture produces a smaller and slower loss of CytOx activity in the deprived blobs (Horton, 1984; Hendry & Jones, 1986; Trusk et al., 1990). Hence, the degree of

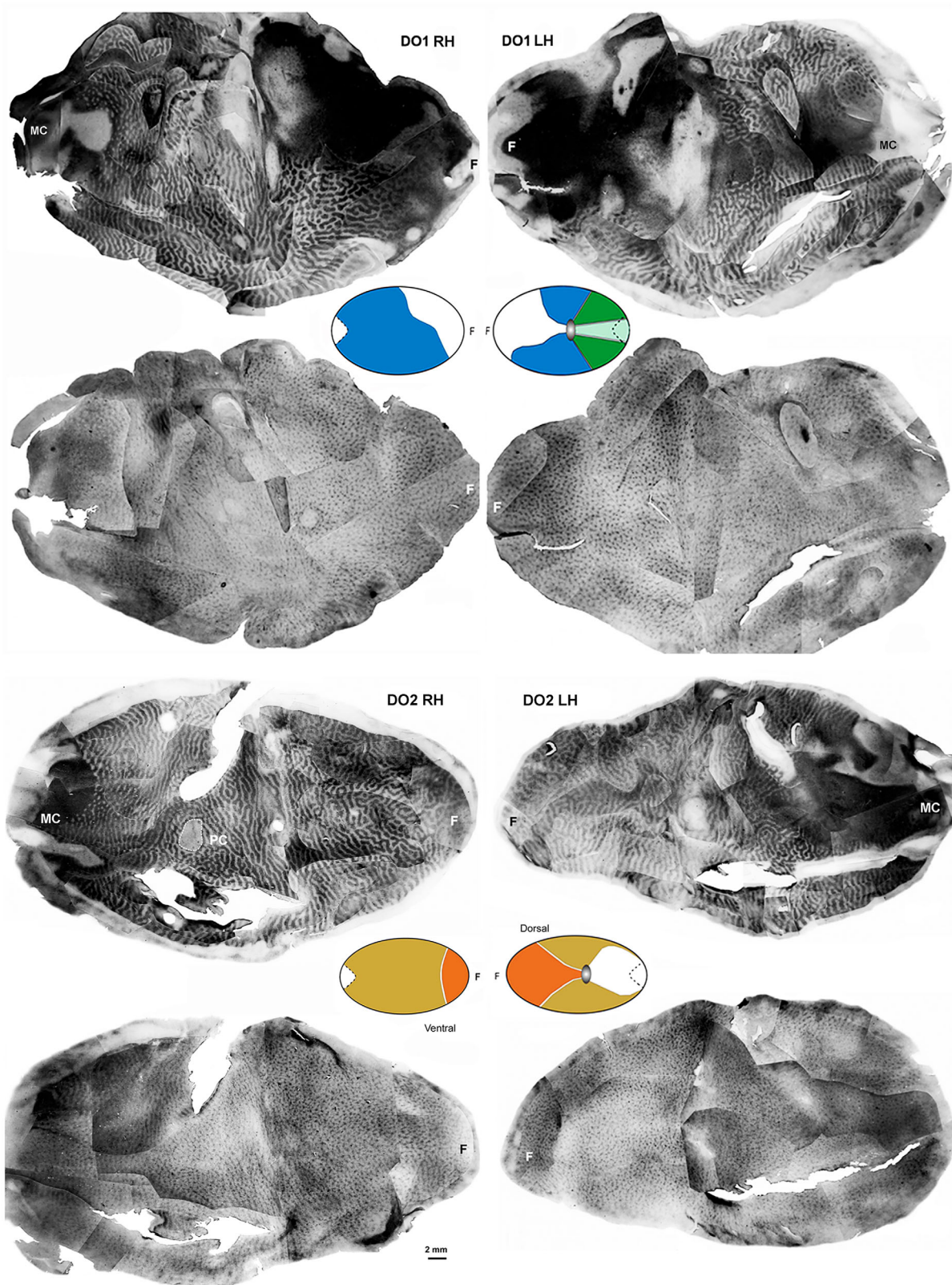


FIGURE 9 Photographic reconstructions of Ocular Dominance Columns in Layer IVc (top) and blobs in Layer III (bottom) of V1 of the right (RH) and left hemispheres (LH) in Cases DO1 and DO2. The small drawing (middle) is a schematic diagram of the lesioned areas in each hemisphere in this case. (F, fovea, MC, monocular crescent). The deafferented regions of the schematic diagram can be correlated with the pattern of ODC in layer IVc (top) [Color figure can be viewed at wileyonlinelibrary.com]

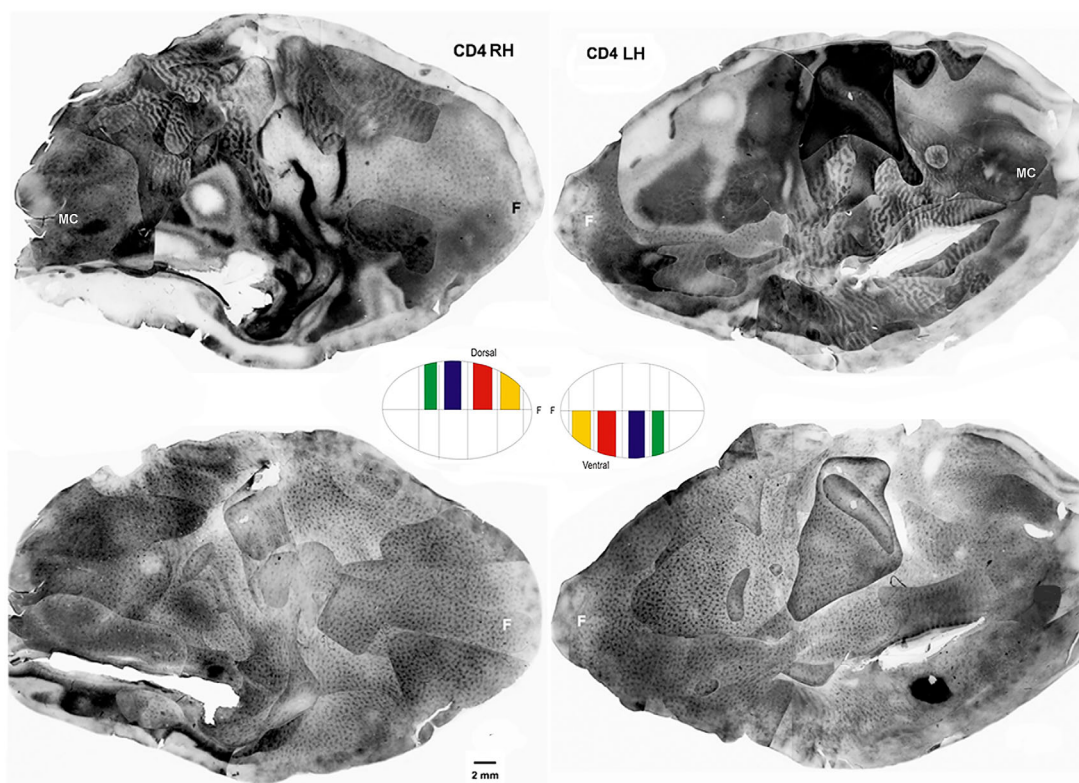


FIGURE 10 Photographic reconstructions of Ocular Dominance Columns in layer IVc (top) and blobs in Layer III (bottom) of V1 of the right (RH) and left hemispheres (LH) in Case CD4. The small drawings (middle) is a schematic diagram of the lesioned areas in this case. (F, fovea, MC, monocular crescent). See also legend for Figure 9 [Color figure can be viewed at wileyonlinelibrary.com]

reduced CytOx activity in the deprived blobs is related to the severity and the duration of the deprivation. There is no evidence of cellular death inside the blobs in any of these three procedures used for sensory deprivation (Trusk et al., 1990). In adult capuchin monkeys, enucleated for 4 and 7 months, not only blobs corresponding to the enucleated eye decrease in size, but blobs corresponding to the intact eye increase their size, compared to the controls (Rosa et al., 1991).

Studies using laser retinal lesions have demonstrated that, in the post-lesion hours, the V1 neurons that originally represented the central area of the lesion become unresponsive (Darian-Smith & Gilbert, 1994; Gilbert & Wiesel, 1992). However, after days or months, cell responsiveness recovers. In cats with retinal laser lesions and subsequent enucleation of the other eye, electrophysiological recordings 2–6 months post-enucleation showed a retinotopic reorganization of V1 (Kaas et al., 1990). In monkeys that received bilateral retinal lesions, it was observed that immediately after the lesions there was a silent, unresponsive zone in V1. However, 75 days after the lesions, half of the cells accounted for in the deprived areas of V1 recovered their responsiveness (Heinen & Skavenski, 1991).

Schmid and colleagues reported that the retinotopic map of V1 in adult cats is capable of reorganizing in a few hours after temporary detachment of the retina or after a laser retinal lesion. The reorganization also happens in cases with monocular deprivation, indicating that lesions of both eyes are not necessary for reorganization (Calford et al., 1999; Schmid et al., 1995, 1996). Botelho et al. (2014)

quantified the capacity for reorganization of the topographic representation of V1 in adult monkeys. Monocular retinal lesions caused a significant reorganization of V1's topographic map, both inside and outside the cortical lesion projection zone. This reorganization was present immediately after monocular retinal lesions, revealing pre-existing subthreshold functional connections of up to 2 mm in V1 that can be rapidly mobilized.

4.1 | Increase in blob size above nondeprived ODCs

In capuchin monkeys with massive retinal lesions to one eye, we observed enlarged CytOx-rich blobs corresponding to the ND ocular dominance stripes that were larger than blobs in the deprived ones, thus confirming the results in macaque (Hess & Edwards, 1987) and humans (Horton & Hedley-White, 1984). Moreover, our data showed that blobs of the intact eye in these same monkeys were larger than blobs from normal controls matched for V1 size (see Figures 11 and 12). We regard this increased size of the blobs in the ND stripes as real. First, blobs in the ND stripes form nearly continuous rows, differing from those in normal ND corresponding portions of V1. Second, Horton's (1984) description of a *M. fascicularis* with a 6-month monocular enucleation indicated that blobs in rows appear larger and semi-confluent. This investigator also noticed that blobs tended to become confluent after long periods of monocular lid suture. Hendry et al. (1988) also observed an increased blob area after a six-month

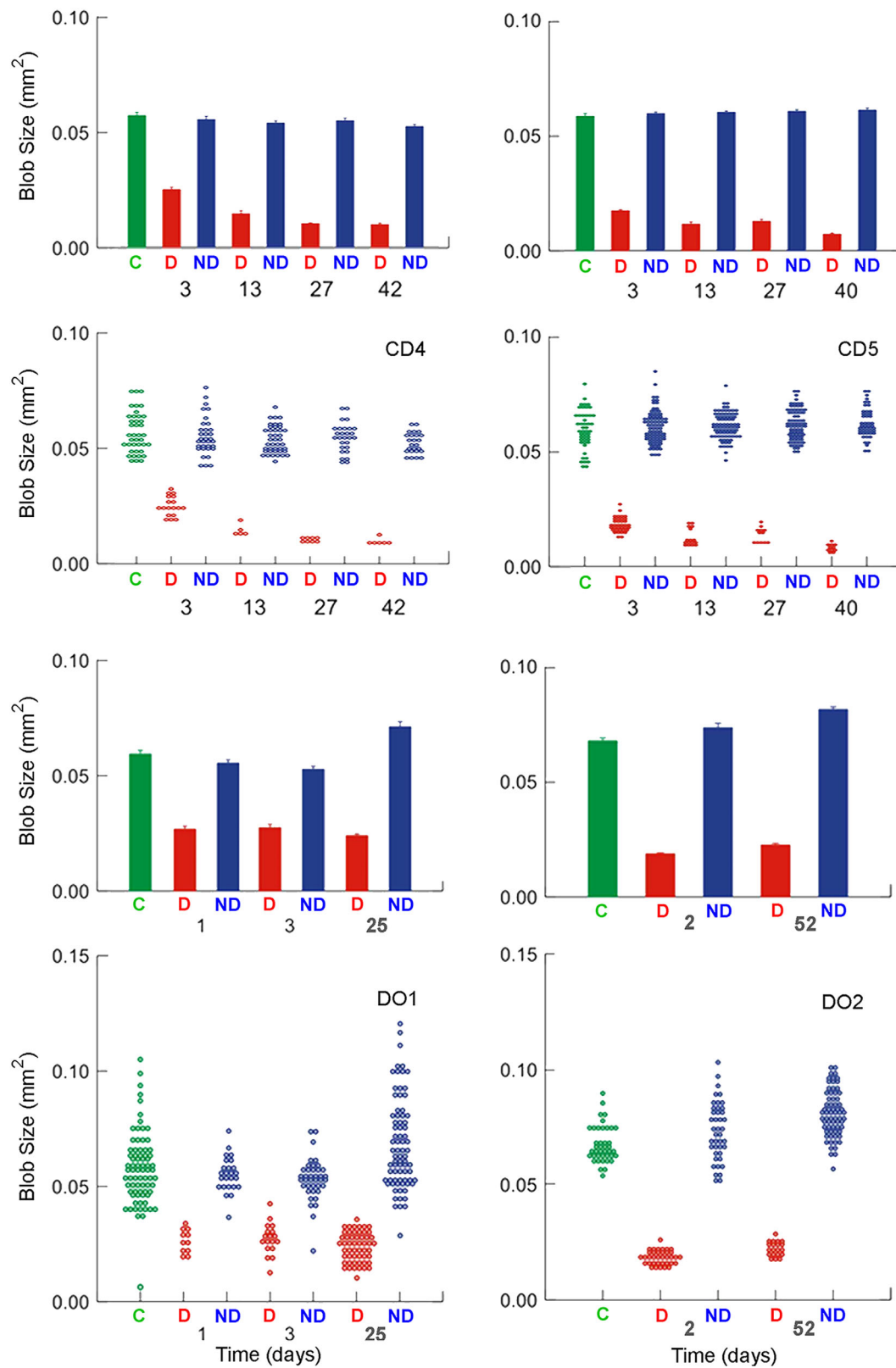


FIGURE 11 Variation of deprived (D) and nondeprived (ND) blob cross-sectional area as a function of the time post-lesion in all cases. The graphs show the mean blob size (top) and the individual size values and the sample dispersion (bottom) in the different lesion times. C, Control areas. Error bars, SEM [Color figure can be viewed at wileyonlinelibrary.com]

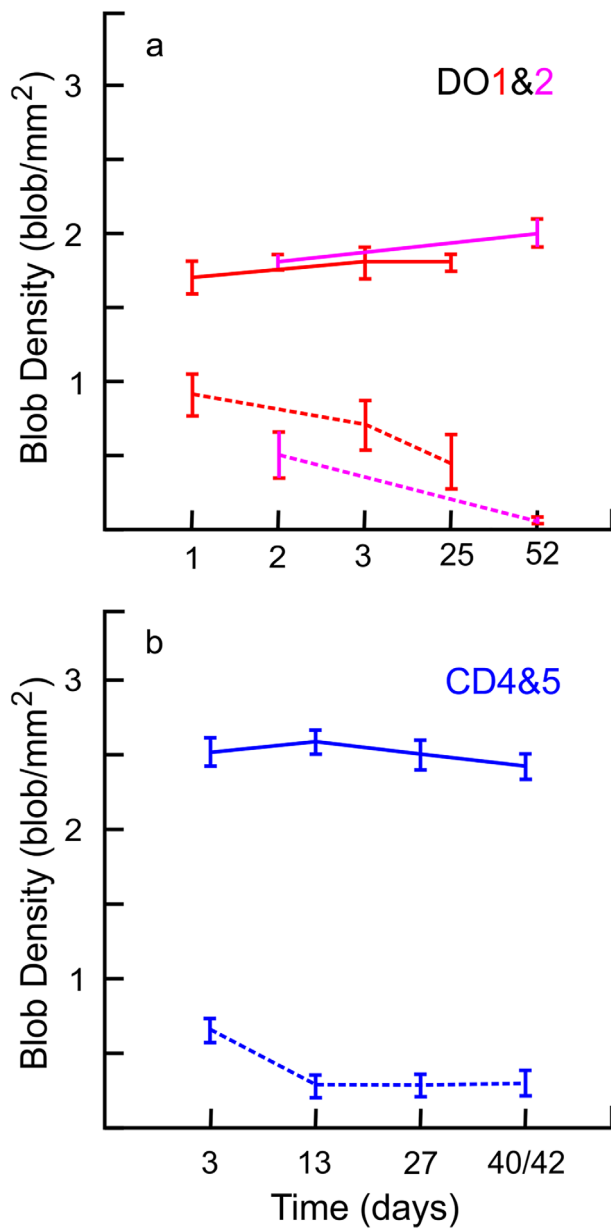


FIGURE 12 Variation of deprived (dashed lines) and ND (solid lines) blob density as a function of the time of the lesions in cases with massive (a) and restricted (b) lesions. Cases DO1 (red) and DO2 (pink) are shown separately (a) because they had distinct times of lesions. The data of Cases CD4 and CD5 (b) were consolidated because they had similar times of lesion [Color figure can be viewed at wileyonlinelibrary.com]

monocular lens removal, but not after 15 days of deprivation with intravitreal TTX injections. Although the latter study attributed this difference to the precise effects of these experimental manipulations, the critical variable may have been, in fact, the survival time. In capuchin monkeys, the shrinkage of the deprived blobs and the increase of blob area were statistically significant relative to that of normal controls. The results achieved in capuchins with retinal laser lesion are in some ways comparable to those reported by Trusk et al. (1990) in macaques submitted to either monocular enucleation or TTX injections. For

example, in all cases, blobs corresponding to the enucleated eye were 50–60% smaller than those corresponding to the intact eye. Blobs along intact-eye ODCs became almost confluent.

4.2 | Blob enlargement versus blob shrinkage

Carrol and Wong-Riley (1984) showed that CytOx reactivity in the blobs of V1 is predominantly localized within dendrites. Later, Wong-Riley and colleagues (1989) showed that the greatest change in neuropil reactivity occurs at the borders of blobs. In this region, axon terminals forming asymmetrical synapses become less densely packed around dendrites after long inactivation times. Wong-Riley et al. (1989) suggested that these terminals might be in part replaced by axonal sprouting of terminals forming symmetrical synapses, which in normal animals contain several highly CytOx-reactive mitochondria. The inter-blob tissue contains neurons responding to both eyes; it is likely that monocular enucleation promotes functional rearrangements in this region as well. In regions immediately outside the ND blobs, terminals of neurons dominated by the enucleated eye may be replaced by terminals of neurons dominated by the intact eye, which would result in an overall increase of CytOx reactivity around the blobs. Thus, enlargement of blobs is likely to be related to plastic mechanisms involving neuropil rather than cell bodies. Recent studies have suggested that the CytOx activity in V1 represents mainly thalamo-cortical afferent terminals that use vesicular glutamate transporter 2 (VGLUT2) as their main glutamate transporter, and cortical dendrites that receive direct inputs from the LGN, instead of reflecting the activity of the somata of cortical neurons (Rockoff et al., 2014; Takahata, 2016).

Trusk et al. (1990) also observed, in macaques submitted to unilateral retinal lesions, increased CytOx reactivity in the inter-blobs

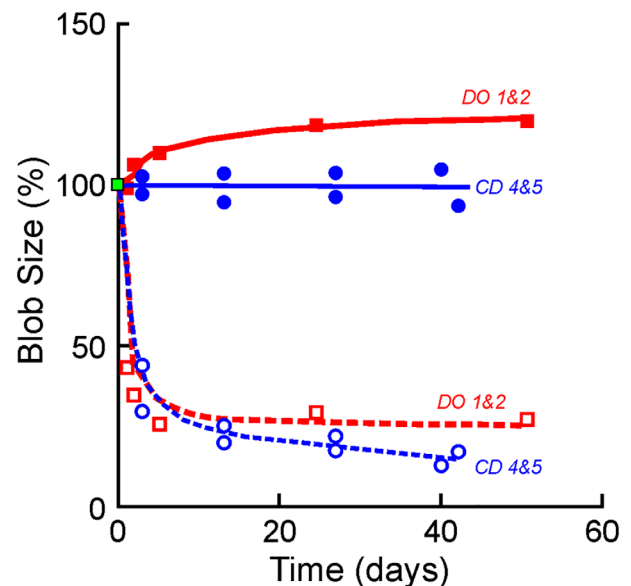


FIGURE 13 Time course of the variation of blob cross-sectional area of deprived (dashed lines) and ND (solid lines) in all cases with restricted (blue) and massive (red) retinal lesions. Different functions were fitted to the data using the method of least squares [Color figure can be viewed at wileyonlinelibrary.com]

overlying the stripes of the undamaged eye, as compared with normal tissue. At the same time, Rosa et al. (1991) showed that deprived and ND monocular crescents show no difference in blob size, a result that contrasts with the marked difference observed between ocular dominance stripes in binocular V1. These results suggest that changes in blob size may result from competition between inputs coming from each eye, rather than from the absolute amount of activity driven by each eye separately.

4.3 | Mechanisms for blob plasticity

The close relationship between the CytOx and the energy needs of the cerebral tissue allowed the use of histochemical methods to evaluate changes in cortical modules in cases of sensory deprivation in the visual system. Studies of significant alterations of the histochemical patterns of this enzyme were mainly accomplished using experimental models for mapping ODC (Horton & Hedley-White, 1984; Wong-Riley & Carroll, 1984; Wong-Riley, 1989; Wong-Riley et al., 1994). Functional reorganization in adult animals, after partial or total sensory or motor deafferentation, was reported by several investigators (Calford et al., 1999, 2003; Chino et al., 1992; Darian-Smith & Gilbert, 1995; Giannikopoulos & Eysel, 2006; Gilbert & Wiesel, 1992; Heinen & Skavenski, 1991; Kaas et al., 1990; Kaas, 1991; LeVay et al., 1980; Rosier et al., 1995; Schmid et al., 1996). Studies of the blob, as a model for plastic changes, were accomplished more systematically by Wong-Riley et al. (1989) and Nie and Wong-Riley (1996). These authors reported a decrease in the amount of gabaergic terminals of inhibitory neurons in the blob. This decrease would cause a release of inhibitory processes in the deafferented areas by altering pre-existing pathways and/or of synapse efficiency in the periblob region. More recent studies have also described a decrease of gamma amino butyric acid (GABA) levels with reduction in the number of inhibitory cell spines and boutons in V1 following a retinal lesion (Arckens et al., 2000; Botelho et al., 2006; Keck et al., 2011). Thus, the functional reorganization after partial or total deafferentation in the visual system would emerge from changes in synaptic efficiency mediated by GABAergic mechanisms (Hendry & Jones, 1986; Hendry et al., 1990, 1994); and, in a second stage, from structural changes possibly mediated by sprouting of collateral axons and/or by the elongation or terminal sprouting of intracortical connections (Darian-Smith & Gilbert 1994; Rosier et al., 1995; Yamahachi et al., 2009). Other studies have also demonstrated changes in the expression of immediate early genes and an upregulation of genes involved in creating the axonal cytoskeleton in the lesion projection zone (Chen et al., 2010; Hu et al., 2009).

We demonstrate that the functional modules represented by the blobs have the capacity of extensive reorganizing with multiple mechanisms after a retinal lesion during adulthood. The results suggest the existence of two separate plastic mechanisms: one of shrinkage of deprived blobs and another, more subtle, of expansion of ND blobs. Plastic changes in blobs described here occur much earlier than previously described.

Further studies are necessary to evaluate the contribution of competition as a basic mechanism to regulate adult plasticity, which results

in sprouting or retraction of axonal processes in ND and deprived territories in the cortex. In addition, the use of immunohistochemical methods to evaluate plastic changes in cortical modules by the expression of calcium binding proteins, GAP-43, synapsin, and GFAP at the level of the primary targets of the ganglion cells (lateral geniculate nucleus and superior colliculus) is the next approach to reveal the molecular mechanisms underlying plastic changes after restricted retinal lesions.

The National Eye Institute (NEI) defines glaucoma as a group of diseases that damage the eye's optic nerve and can result in vision loss and blindness. Chronically high blood sugar from diabetes is associated with damage to the tiny blood vessels in the retina, leading to diabetic retinopathy. Diabetic retinopathy can cause blood vessels in the retina to leak fluid or hemorrhage, distorting vision (NEI). Massive and restricted retinal lesions cause damage in the primary visual cortex that appears to be comparable with the conditions present in glaucoma and diabetic retinopathy. Lesions of glaucoma destroy fibers of the optic disc and produce a profound loss of peripheral vision and impairment of depth perception. Early diabetic retinopathy is less severe and is usually asymptomatic. We regard our massive and restricted lesions as simulating these two clinical disorders, respectively.

ACKNOWLEDGMENTS

We wish to thank Edil Saturato da Silva Filho and Liliane Herringer Motta for their skillful technical assistance.

In Memoriam of Vivien Casagrande

Vivien Alice Casagrande made fundamental contributions to the significance of cytochrome oxidase blobs of V1 and in comparative studies of their distribution in primates. Her enthusiasm, scientific expertise and rigorous application of neuroanatomical techniques have greatly influenced this field of research. In our hearts, she will be very much missed!

CONFLICT OF INTEREST

We declare that there is no conflict of interest, either financial, personal, or other relationships with other people or organizations within three years of beginning the submitted work that could inappropriately influence the results or interpretation of the data of the article.

AUTHOR CONTRIBUTIONS

All authors had full access to all the data in the study and take responsibility for the integrity of the data and the accuracy of the data analysis. MFF, RG, and LGU planned the experiments. MFF, SSP, JMS, AKJA and RG executed the experiments, and discussed the data. RG, MFF, and JMS wrote the manuscript and prepared the illustrations. RG and LGU reviewed the data and revised the manuscript.

ORCID

Ricardo Gattass  <http://orcid.org/0000-0002-0321-1490>

REFERENCES

- Arckens, L., Schweigart, G., Qu, Y., Wouters, G., Pow, D. V., Vandesande, F., ... Orban, G. A. (2000). Cooperative changes in GABA, glutamate and activity levels: the missing link in cortical plasticity. *European Journal of Neuroscience*, 12, 4222–4232.
- Barsante, C., & Diniz, A. V. (1997). Xenônio x Argon x Criptônio x Diode. In João Alberto Holanda de Freitas & Jacqueline Provenzano (Eds.), *Laser in ophthalmology* (pp. 89–97). Rio de Janeiro.
- Botelho, E. P., Soares, J. G. M., Pereira, S. S., Fiorani, M., & Gattass, R. (2006). Distribution of calbindin-28kD and parvalbumin in V1 in normal adult *Cebus apella* monkeys and in monkeys with retinal lesions. *Brain Research*, 1117, 1–11.
- Botelho, E. P., Ceriatte, C., Soares, J. G. M., Gattass, R., & Fiorani, M. (2014). Quantification of early stages of cortical reorganization of the topographic map of V1 following retinal lesions in monkeys. *Cerebral Cortex*, 24, 1–16.
- Bozini, D. G. (1997). Physical Principles of Laser. In Alberto Holanda de Freitas & Jacqueline Provenzano (Eds.), *Laser in Ophthalmology* (pp. 1–18). Rio de Janeiro.
- Calford, M. B., Schmid, L. M., & Rosa, M. G. P. (1999). Monocular focal retinal lesions induce short-term topographic plasticity in adult cat visual cortex. *Proceedings of Biological Sciences*, 266, 499–507.
- Calford, M. B., Wright, L. L., Metha, A. B., & Taglianetti, V. (2003). Topographic plasticity in primary visual cortex is mediated by local cortico-cortical connections. *Journal of Neuroscience*, 23, 6434–6442.
- Carroll, E.W. & Wong-Riley, M.T. (1984). Quantitative light and electron microscopic analysis of cytochrome oxidase-rich zones in the striate cortex of the squirrel monkey. *Journal of Comparative Neurology*, 222: 1–17.
- Chen, J., Yamahachi, H., & Gilbert, C. D. (2010). Experience-dependent gene expression in adult visual cortex. *Cerebral Cortex*, 20, 650–660.
- Chino, Y. M., Kaas, J. H., Smith, E. L., III, Langston, A. L., & Cheng, H. (1992). Rapid reorganization of cortical maps in adult cats following restricted deafferentation in retina. *Vision Research*, 32, 789–796.
- Darian-Smith, C., & Gilbert, C. D. (1994). Axonal sprouting accompanies functional reorganization in adult cat striate cortex. *Nature*, 368, 737–740.
- Darian-Smith, C., & Gilbert, C. D. (1995). Topographic reorganization in the striate cortex of the adult cat and monkey is cortically mediated. *Journal of Neuroscience*, 15, 1631–1647.
- Farias, M. F., Gattass, R., Piñón, M. C., & Ungerleider, L. G. (1997). Tangential distribution of cytochrome oxidase-rich blobs in the primary visual cortex of macaque monkeys. *Journal Comparative Neurology*, 386, 217–228.
- Gattass, R., Souza, A. P. B., & Rosa, M. G. P. (1987). Visual topography in V1 in the *Cebus* monkey. *Journal Comparative Neurology*, 259, 529–548.
- Giannikopoulos, D. V., & Eysel, U. T. (2006). Dynamics and specificity of cortical map reorganization after retinal lesions. *Proceedings of the National Academy of Science United States of America*, 103, 10805–10810.
- Gilbert, C. D., & Wiesel, T. N. (1992). Receptive field dynamics in adult primary visual cortex. *Nature*, 356, 150–152.
- Heinen, S. J., & Skavenski, A. A. (1991). Recovery of visual responses in foveal V1 neurons following bilateral foveal lesions in adult monkey. *Experimental Brain Research*, 83, 670–674.
- Hendrickson, A. E. (1985). Dots, stripes and columns in monkey visual cortex. *Trends in Neuroscience*, 8, 406–410.
- Hendry, S. H. & Jones, E. G. (1986). Reduction in number of immunostained GABAergic neurones in deprived-eye dominance columns of monkey area 17. *Nature*, 320, 750–753.
- Hess, D. T. & Edwards, M. A. (1987). Anatomical demonstration of ocular segregation in the retinogeniculocortical pathway of the New World capuchin monkey (*Cebus apella*). *Journal of Comparative Neurology*, 264, 409–420.
- Hendry, S. H., Jones, E. G. & Burstein, N. (1988). Activity-dependent regulation of tachykinin-like immunoreactivity in neurons of monkey visual cortex. *Journal of Neuroscience*, 8, 1225–1238.
- Hendry, S. H., Fuchs, J., deBlas, A. L. & Jones, E. G. (1990). Distribution and plasticity of immunocytochemically localized GABAA receptors in adult monkey visual cortex. *Journal of Neuroscience*, 10, 2438–2450.
- Hendry, S. H., Huntsman, M. M., Viñuela, A., Möhler, H., de Blas, A. L. & Jones, E. G. (1994). GABAA receptor subunit immunoreactivity in primate visual cortex: distribution in macaques and humans and regulation by visual input in adulthood. *Journal of Neuroscience*, 14, 2383–2401.
- Horton, J. C., & Hubel, D. H. (1981). Regular patchy distribution of cytochrome oxidase staining in primary visual cortex of macaque monkey. *Nature*, 292, 762–776.
- Horton, J. C. (1984). Cytochrome oxidase patches: A new cytoarchitectonic feature of monkey visual cortex. *Philosophical Transactions of the Royal Society London, B - Biological Sciences*, 304, 199–253.
- Horton, J. C., & Hedley-White, E. T. (1984). Mapping of cytochrome oxidase patches and ocular dominance columns in human visual cortex. *Philosophical Transactions of the Royal Society London, B - Biological Sciences*, 304, 255–272.
- Hu, T. T., Laeremans, A., Eysel, U. T., Cnops, L., & Arckens, L. (2009). Analysis of c-fos and zif268 expression reveals time-dependent changes in activity inside and outside the lesion projection zone in adult cat area 17 after retinal lesions. *Cerebral Cortex*, 19, 2982–2992.
- Kaas, J. H. (1991). Plasticity of sensory and motor maps in adult mammals. *Annual Review of Neuroscience* 14, 137–167.
- Kaas, J. H., Krubitzer, L. A., Chino, Y. M., Langston, A. L., Polley, E. H., & Blair, N. (1990). Reorganization of retinotopic cortical maps in adult mammals after lesions of the retina. *Science*, 248, 229–231.
- Keck, T., Scheuss, V., Jacobsen, R. I., Wierenga, C. J., Eysel, U. T., Bonhoeffer, T., & Hübener, M. (2011). Loss of sensory input causes rapid structural changes of inhibitory neurons in adult mouse visual cortex. *Neuron*, 71, 869–882.
- Lachica, E. A., Beck, P. D., & Casagrande, V. A. (1992). Parallel pathways in macaque monkey striate cortex: Anatomically defined columns in layer III. *Proc Natl Acad Sci USA*, 89, 3566–3570.
- LeVay, S., Wiesel, T. N., & Hubel, D. H. (1980). The development of ocular dominance columns in normal and visually deprived monkeys. *Journal Comparative Neurology*, 191, 1–51.
- LeVay, S., Connolly, M., Houde, J., & Van Essen, D. C. (1985). The complete pattern of ocular dominance stripes in the striate cortex and visual field of the macaque monkey. *Journal of Neuroscience*, 5, 486–501.
- Livingstone, M. S., & Hubel, D. H. (1982). Thalamic inputs to cytochrome oxidase-rich regions in monkey visual cortex. *Neurobiology*, 79, 6098–6101.
- Marcondes, M., Rosa, M. G. P., Fiorani, M., Lima, B., & Gattass, R. (2018). Distribution of cytochrome oxidase-rich patches in human primary visual cortex. *Journal Comparative Neurology*, 526, current issue.
- Medeiros, H. A. G. (1997). Lentes utilizadas em fotocoagulação. In João Alberto Holanda de Freitas & Jacqueline Provenzano (Eds.), *Laser in Ophthalmology* (pp. 103–109). Rio de Janeiro.
- Nie, F. & Wong-Riley, M. T. (1996). Metabolic and neurochemical plasticity of gamma-aminobutyric acid-immunoreactive neurons in the adult

- macaque striate cortex following monocular impulse blockade: quantitative electron microscopic analysis. *Journal of Comparative Neurology*, 370, 350–366.
- Rockoff, E. C., Balaram, P., & Kaas, J. H. (2014). Patchy distributions of myelin and vesicular glutamate transporter 2 align with cytochrome oxidase blobs and interblobs in the superficial layers of the primary visual cortex. *Eye Brain*, 6, 19–27.
- Rosa, M. G. P., Gattass, R., & Fiorani, M. Jr. (1988). Complete pattern of ocular dominance stripes in V1 of a New World monkey, *Cebus apella*. *Experimental Brain Research*, 72, 645–648.
- Rosa, M. G. P., Gattass, R., & Soares, J. G. M. (1991). A quantitative analysis of cytochrome oxidase-rich patches in primary visual cortex of *Cebus* monkeys: Topographic distribution and effects of late monocular enucleation. *Experimental Brain Research*, 84, 195–209.
- Rosa, M. G. P., Gattass, R., Fiorani, M., Jr., & Soares, J. G. M. (1992). Laminar, columnar and topographic aspects of ocular dominance in the primary visual cortex of *Cebus* monkeys. *Experimental Brain Research*, 88, 249–264.
- Rosier, A. M., Arckens, L., Demeulemeester, H., Orban, G. A., Eysel, U. T., Wu, Y. J., & Vandesande, F. (1995). Effect of sensory deafferentation on immunoreactivity of GABAergic cells and on GABA receptors in the adult cat visual cortex. *Journal Comparative Neurology*, 359, 476–489.
- Schmid, L. M., Rosa, M. G. P., & Calford, M. B. (1995). Retinal detachment induces massive immediate reorganization in visual cortex. *NeuroReport*, 6, 1349–1353.
- Schmid, L. M., Rosa, M. G. P., Calford, M. B., & Ambler, J. S. (1996). Visuotopic reorganization in the primary visual cortex of adult cats following monocular and binocular retinal lesions. *Cerebral Cortex*, 6, 388–405.
- Silvermann, M. S., & Tootell, R. G. H. (1987). Modified technique for cytochrome oxidase histochemistry: Increased staining intensity and compatibility with 2-deoxyglucose autoradiography. *Journal of Neuroscience Methods*, 19, 1–10.
- Takahata, T. (2016). What does cytochrome oxidase histochemistry represent in the visual cortex?. *Frontiers in Neuroanatomy*, 10, 79.
- Tootell, R. B., Hamilton, S. L. & Silverman, M. S. (1985). Topography of cytochrome oxidase activity in owl monkey cortex. *Journal of Neuroscience*, 5, 2786–2800.
- Tootell, R. B. & Silverman, M. S. (1985). Two methods for flat-mounting cortical tissue. *Journal of Neuroscience Methods*, 15, 177–190.
- Trusk, T. C., Kaboord, W. S., & Wong-Riley, M. T. T. (1990). Effects of monocular enucleation, tetrodotoxin, and lid suture on cytochrome oxidase reactivity in supragranular puffs of adult Macaque striate cortex. *Visual Neuroscience*, 4, 185–204.
- Wong-Riley, M. T. T. (1979). Changes in the visual system of monocularly sutured or enucleated cats demonstrable with cytochrome oxidase histochemistry. *Brain Research*, 171, 11–28.
- Wong-Riley, M. T. T., & Carroll, E. W. (1984). Effect of impulse blockage on cytochrome activity in monkey visual system. *Nature*, 307, 262–264.
- Wong-Riley, M. T. T., Trusk, T., Tripathi, S., & Hoppe, D. (1989). Effect of retinal impulse blockage on cytochrome oxidase-rich zones in the macaque striate cortex, II: Quantitative EM analysis of neuropil. *Visual Neuroscience*, 2, 499–514.
- Wong-Riley, M. T., Trusk, T. C., Kaboord, W. & Huang, Z. (1994). Effect of retinal impulse blockage on cytochrome oxidase-poor interpuffs in the macaque striate cortex: quantitative EM analysis of neurons. *Journal of Neurocytology*, 23, 533–553.
- Yamahachi, H., Marik, S. A., McManus, J. N., Denk, W., & Gilbert, C. D. (2009). Rapid axonal sprouting and pruning accompany functional reorganization in primary visual cortex. *Neuron*, 64, 719–729.

How to cite this article: Farias MF, Ungerleider LG, Pereira SS, Amorim AKJ, Soares JGM, Gattass R. Time course of cytochrome oxidase blob plasticity in the primary visual cortex of adult monkeys after retinal laser lesions. *J Comp Neurol*. 2018;00:1–14. <https://doi.org/10.1002/cne.24434>